

**Investigation of Organic Inhibitor on Mild Steel using In Situ Atomic Force Microscopy and Electrochemical Measurement**

H. Wang, B. Brown, S. Nestic  
Institute for Corrosion Multiphase Technology, Ohio University  
342 West State Street  
Athens, OH 45701  
USA

A. Pailleret  
Sorbonne Université, CNRS, Laboratoire Interfaces et Systèmes Electrochimiques (LISE, UMR 8235)  
4 place Jussieu, (case courrier 133)  
Paris, 75005  
France

**ABSTRACT**

Corrosion inhibition is an essential tool for assuring asset integrity in oil and gas transportation. Consequently, research related to organic surfactant-type inhibitors, which adsorb on a metal surface to form a protective layer against corrosion, is of great interest to the oil and gas industry. Conventional thinking, as conceptualized in the open literature, has the decrease in corrosion rates due to inhibitor addition directly related to surface coverage. However, research studies have so far not provided direct evidence of such a link; this is primarily due to the limitations of conventional electrochemical techniques used to investigate them. In the present research, in situ atomic force microscopy (AFM) coupled with electrochemical measurements has been used to study surface coverage by a tetradecyldimethylbenzylammonium inhibitor model compound; it possesses 14 carbon atoms in its hydrophobic tail (Q-C14). Application of AFM elucidates physical attributes of the inhibitor adsorption morphology and provides information which cannot be obtained by traditional electrochemical techniques alone. Analysis of AFM data indicates that the adsorbed inhibitor film likely exists as a self-assembled layer. AFM imaging results showed that the surface coverage on mild steel was closely related to inhibitor bulk solution concentration. When the bulk solution inhibitor concentration was below the surface saturation value, AFM measurements indicated partial coverage of the surface by the inhibitor film and patchy corrosion of the metal surface was observed; this has the potential to result in localized attack. When inhibitor bulk concentration was above the surface saturation value, full surface coverage was detected by AFM measurements and corrosion was uniformly retarded.

**Key words:** corrosion inhibitor, organic surfactant, quaternary ammonium, carbon steel, in-situ atomic force microscopy, CO<sub>2</sub> corrosion

## INTRODUCTION

In oil and gas production systems, carbon steel has been used widely as pipeline materials during transport and storage of crude oils and derived petroleum products.<sup>1</sup> Although carbon steel has excellent mechanical properties and low cost, its susceptibility to corrosion attack in a typical service environment containing some water, has caused economic and environmental losses.<sup>2</sup> Organic surfactants, which often contain nitrogen, oxygen and sulfur atoms as well as multiple bonds that assist with adsorption, exhibit excellent inhibition effect at very low concentrations (ppm level) and are commonly employed as corrosion inhibitors on mild steel.<sup>3</sup>

The corrosion inhibition efficiency of organic inhibitors is associated with their adsorption properties, which depend on the chemical reactivity of the metal-solution interface, surfactant chemistry, and also bulk inhibitor concentration.<sup>4</sup> It is critical to understand the influence of the latter on adsorption structure and surface coverage for a better understanding of the corrosion inhibition mechanism. Some of the current research on corrosion inhibitors has focused on investigating the influence of electrochemical reactions mechanisms at metal-solution interfaces.<sup>5</sup> However, such research is only rarely able to connect inhibitor adsorption behavior on metallic surfaces with inhibition mechanisms due to the limitation of conventional electrochemical techniques.<sup>6</sup> These traditional electrochemical methods can only obtain corrosion rates averaged over the whole surface and are not able to provide information about localized adsorption. The application of AFM techniques can fill in this gap and accomplish imaging of the inhibitor adsorption structures on various substrates, including metallic surfaces.

Although there are limited AFM studies on molecular inhibitor research in the field of corrosion, the adsorption of organic surfactants (especially quaternary ammonium) on mica has been extensively studied by AFM imaging. These studies indicated that variations in surfactant chemistry, such as the alkyl tail length, counter ion type,<sup>7</sup> and head-group structure,<sup>7, 8</sup> have significant influence on adsorption morphology, which varies from spherical micelles, meandering cylindrical micelles to featureless bilayers. Molecular simulation research on surfactant adsorption also confirms that both the head group size and hydrophobic interaction coefficients can affect the adsorption morphology.<sup>9, 10</sup> These AFM and molecular simulation studies<sup>7-10</sup> with organic surfactants provided valuable background knowledge for developing an effective methodology on molecular inhibitor adsorption research.

The AFM imaging of adsorbed molecular inhibitor layers can provide us with information about how the surfactant chemistry and surface reactivity of the substrate influence the adsorption structure. In addition, AFM images can also be used to investigate the evolution of surfactant surface coverage. For example, J. T. Woodward *et al.*<sup>11</sup> studied the growth kinetics of octadecylphosphonic acid based self-assembled monolayers (SAM) on mica by AFM imaging of an incomplete film. The formation of patchy adsorbed surfactant islands was observed by AFM on mica surface. It was found to follow a sequence of nucleation, growth, and coalescence, which finally resulted in a submonolayer.<sup>11</sup> The surface coverage obtained below saturated bulk concentration of octadecylphosphonic acid could be captured by AFM imaging and presented as a function of immersion time. Two typical adsorption kinetics models were compared with the surface coverage data, and the fitting results indicate that growth kinetics of patchy covered islands was consistent with the interfacial diffusion-limited kinetics rather than with the adsorption limited (Langmuir) kinetics. However, AFM research of fractal aggregation<sup>12</sup> suggested that the diffusion-limited micellization kinetics model fits less with the evolution of isolated structures.<sup>12</sup> Meanwhile, similar AFM studies of sub-monolayer formation confirmed the nucleation and coalescence process of surfactant islands, but a different kinetic theory focused on 2D cluster growth was proposed.<sup>13</sup> In another contribution, AFM investigations of octadecyltrimethylammonium bromide adsorption on mica revealed that, initially, there is a rapid and random adsorption. After this first stage, the surface coverage increases significantly with the formation of a self-assembled two-phase film for times longer than 24 hours.<sup>14</sup>

Most AFM studies about surfactant adsorption morphology and surface coverage effects are performed on a mica surface. Although similar adsorption behavior has been observed on an inert metallic surface such as gold,<sup>15, 16</sup> there are very few AFM studies of surfactant adsorption on carbon steel surfaces due to the dramatic alteration of interfacial properties and adsorption mechanisms by the corrosion processes.

However, it is crucial to use carbon steels as substrates in order to investigate inhibitor efficiency. In this work, an in-situ AFM technique together with electrochemical measurements were applied to study the influence of bulk inhibition concentration on the inhibitor surface coverage of UNS G10180 carbon steel.

## EXPERIMENTAL PROCEDURE

### 2.1 Synthesis of Corrosion Inhibitor Model Compounds

In order to obtain the required purity, a model corrosion inhibitor was synthesized by our group.<sup>17</sup> The model compounds used in this work consisted of a polar head group, dimethylbenzylammonium, and a hydrophobic tail: Tetradecyl ( $-C_{14}H_{17}$ ), as shown in Figure 1. The synthesis reaction is illustrated in Figure 2.<sup>18</sup> Proton nuclear magnetic resonance ( $^1H$ -NMR) spectroscopy was used to characterize the synthesized model compounds, indicating 99% of purity. The detailed characterization procedure has been illustrated in a previous publication.<sup>18</sup>

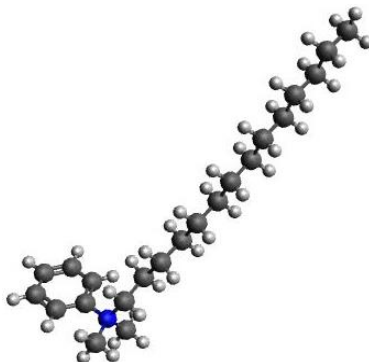


Figure 1: The molecular microstructure of tetradecylbenzyltrimethylammonium (Q-C14).

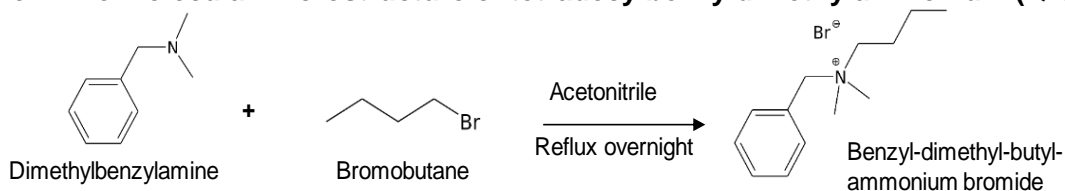


Figure 2: Reaction for synthesizing model compound alkylbenzyltrimethylammonium.

### 2.2 Materials and solutions

The steel specimen were cut from a pipeline sample made of UNS G10180 carbon steel, and then successively polished using 400, 600, 800, and 1200 grit silicon carbide papers followed by 9, 3, and 1  $\mu m$  diamond particles. The samples were then washed with acetone, ethanol, and water and dried in air.

The bulk inhibitor concentration was selected on the basis of its critical micellar concentration (CMC): 0 ppm, 25 ppm (0.5 CMC), 50 ppm (1 CMC) and 100 ppm (2 CMC). The CMC of Q-C14 was obtained by measuring changes in surface tension with concentration using the DuNoy ring method with a Kruss<sup>†</sup> tensiometer. Solutions of 1 wt% NaCl containing Q-C14 were prepared using deionized water with a conductivity of 18  $M\Omega \cdot cm^{-1}$ . The solution was deoxygenated by sparging  $CO_2$  for at least 2 hours before beginning the experiments, and  $CO_2$  was continuously purging during the entire test. Testing was conducted at room temperature (25  $^{\circ}C$ ), and the initial pH of the test solution was pH 4. The test matrix is shown in Table 1.

<sup>†</sup> Trade Name

**Table 1**  
**Experimental Conditions**

Q-C14 (Quaternary ammonium, CMC: 50 ppm) in 1%wt NaCl aqueous solutions, CO <sub>2</sub> saturated, 25 °C, initial pH : 4			
Material	Concentrations	Technique	Reproducibility
UNS G10180 carbon steel	0 CMC (0 ppm)	Imaging In situ LPR	5 tests
	0.5 CMC (25 ppm)		6 tests
	1 CMC (50 ppm)		3 tests
	2 CMC (100 ppm)		3 tests

### 2.3 AFM measurements

AFM measurements were carried out in situ in aqueous solutions containing various concentrations of inhibitor. AFM imaging experiments were performed using the commercial Keysight<sup>‡</sup> Scanning Probe Microscope system in contact mode. Measurements were made at the carbon steel-aqueous solution interface in order to determine the surface coverage. The scan rate was set to 8000 nm/s for optimized imaging on UNS G10180 carbon steel, and the scan area was 10 μm<sup>2</sup>. A resolution of 512 by 512 pixels was adopted for all AFM images. AFM tips made of silicon were mounted on triangular cantilevers with nominal spring constants of 0.3 N/m. Inhibitor layers can be imaged repeatedly without causing tip-induced damage using a low load (< 2 nN). However, inhibitors can also be scratched off of the substrate surface when desired by repeatedly scanning the film at much higher operating normal forces.<sup>19</sup> The detailed procedure of scratching experiments has been illustrated in our group's previous work.<sup>20</sup>

### 2.4 In situ LPR measurements

A custom-made AFM sample holder with a three-electrode cell configuration (shown in Figure 3) was used in this study. AISI 316L stainless steel was used as a counter electrode and UNS G10180 carbon steel was used as the working electrode. The reference electrode was a 3mL small cell with built-in Ag wire in AgCl saturated KCl solution.<sup>21</sup> Linear polarization resistance (LPR) was used to obtain corrosion rates by polarizing the working electrode from -10 mV to +10 mV w.r.t. the corrosion potential at a scan rate of 1.25 mV/s. A value of B = 26 mV/decade was used to convert the polarization resistance into a corrosion current and corrosion rate based on a previous mechanistic study of CO<sub>2</sub> corrosion in inhibited systems.<sup>22</sup> In this study changes of corrosion information such as Tafel slopes and corrosion rates due to addition of inhibitor were recorded by electrochemical frequency modulation technique.<sup>22</sup>

---

<sup>‡</sup> Trade Name

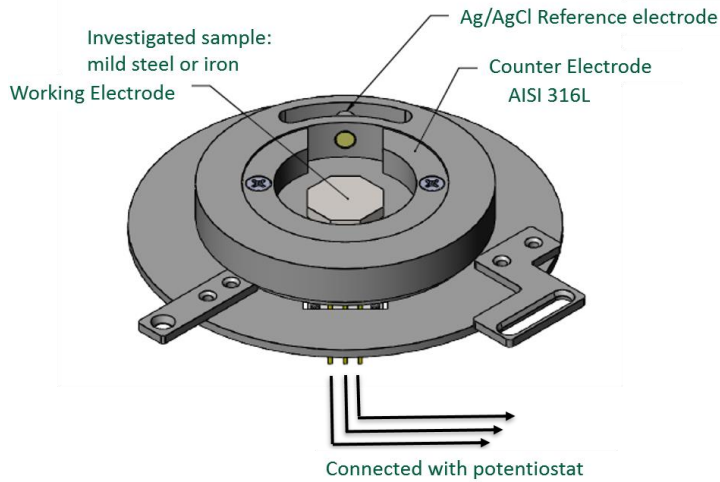


**Figure 3: Custom-made sample holder for in-situ electrochemical AFM experiments**

## RESULTS

### LPR corrosion rates measurements

Figure 4 shows the LPR corrosion rate measurements of UNS G10180 steel in 1 wt% NaCl solution at different times for various Q-C14 inhibitor bulk concentrations. One can first observe that, whatever the concentration, the corrosion rate initially diminishes drastically with time before it levels off at a relatively constant value for the duration of the test. It is thought that during the initial phase, Q-C14 adsorbs progressively on the steel surface, leading to an increase in the surface coverage and therefore to a more efficient inhibition of corrosion. The constant corrosion rate value reached after longer exposure decreases with Q-C14 inhibitor bulk concentration. This agrees with Hackerman *et al.* theory showing that the amount of adsorbed inhibitor on the metal surface reaches a maximum at a certain bulk solution concentration, called surface saturation concentration in this theory.<sup>23, 24</sup> No more adsorption should be expected after reaching saturated concentration, indicating that corrosion rates will not decrease further.

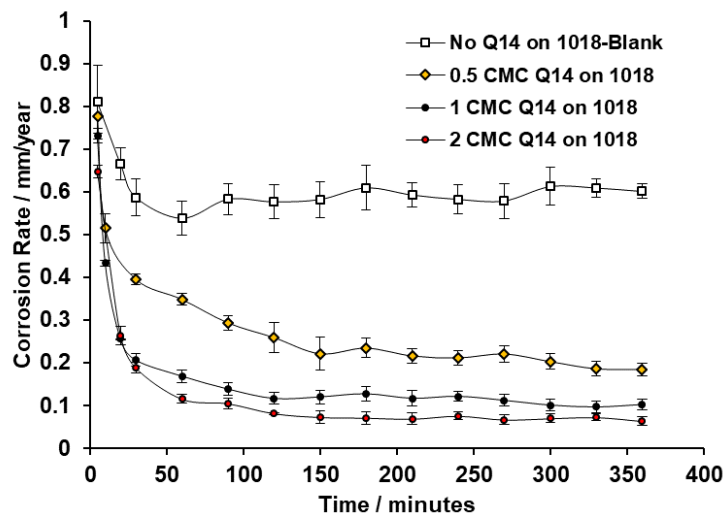


**Figure 4. LPR corrosion rates of UNS G10180 in 1 wt% NaCl solution with various inhibitor concentrations.**

## Real time monitoring of steel surface morphology in the absence of inhibitor

The time-dependent morphology change of the steel surface immersed in uninhibited 1wt% NaCl aqueous solution is presented in Figure 5. Figure 5a shows the image of untreated mild steel substrate before it is exposed to the solution. Only polishing lines can be observed on the surface when the steel was imaged in air. Figure 5b shows the morphology of the UNS G10180 steel surface after 10 minutes immersion in 1wt% NaCl in the absence of inhibitors. It can be seen that the steel surface immediately displays some new features, i.e. areas that are relatively higher than the surrounding surface.

These newly formed structures are cementite structures ( $\text{Fe}_3\text{C}$ ) which is an integral part of the steel and is revealed due to corrosion leading to a rapid dissolution of the surrounding ferritic matrix. The UNS G10180 has a bi-phased ferrite + pearlite microstructure,<sup>25</sup> wherein pearlite is a two-phase structure with lamellar cementite situated in a ferrite matrix,<sup>26, 27</sup> forming a well-distributed network in the steel. From a corrosion point of view, the  $\text{Fe}_3\text{C}$  present in pearlite phase is more noble than the ferrite phase ( $\alpha$  - Fe) and remains inert, and acts as a cathodic site for the hydrogen evolution process.<sup>28</sup> As a consequence, iron dissolves preferentially from ferrite phase (or matrix), leaving the cathodic region (lamellar  $\text{Fe}_3\text{C}$ ) intact,<sup>29, 30</sup> which is shown on AFM images as elevated areas (Figure 5b).

With prolonged immersion (images provided in Figure 5c and Figure 5d for one hour and four hours) polishing lines originally seen on the steel surface gradually disappear. The average height difference between inert cementite and corroded surrounding ferrite phases increases with immersion time since ferrite dissolves continuously. According to the topography profiles in Figure 5 b-d, the height difference between pearlite structure and surrounding ferrite is about  $20 \text{ nm} \pm 10 \text{ nm}$  after immersion in the corrosive solution for 10 minutes, whereas after 1 hour immersion, this height difference becomes about  $90 \pm 30 \text{ nm}$ . Finally, when adding the uninhibited 1wt% NaCl aqueous solution about 4 hours later, the height difference is about  $240 \pm 50 \text{ nm}$ .

Assuming that the height difference between inert cementite regions and corroded ferrite can be interpreted as a measure of the time averaged local corrosion rate, it is estimated from surfaces profiles in Figure 5b and 5c and equation (1) that the corrosion rate between 10 minutes to 1 hour is  $0.74 \pm 0.21 \text{ mm/year}$ . Similarly from Figure 5c and 5d the time averaged local corrosion rate from 1 hour to 4 hours exposure is estimated as  $0.44 \pm 0.23 \text{ mm/year}$ , which is in the range of the surface averaged corrosion rate as measured by LPR of  $0.61 \pm 0.1 \text{ mm/year}$ .

$$\begin{aligned} & (90\text{nm} \pm 30 - 20\text{nm} \pm 10)/50 \text{ mins} * 60(\text{min/hr}) * 24(\text{hr/day}) * 365(\text{day/year})/10^6(\text{nm/mm}) = \\ & \qquad \qquad \qquad 0.74 \pm 0.21\text{mm/year} \qquad \qquad \qquad (1) \end{aligned}$$

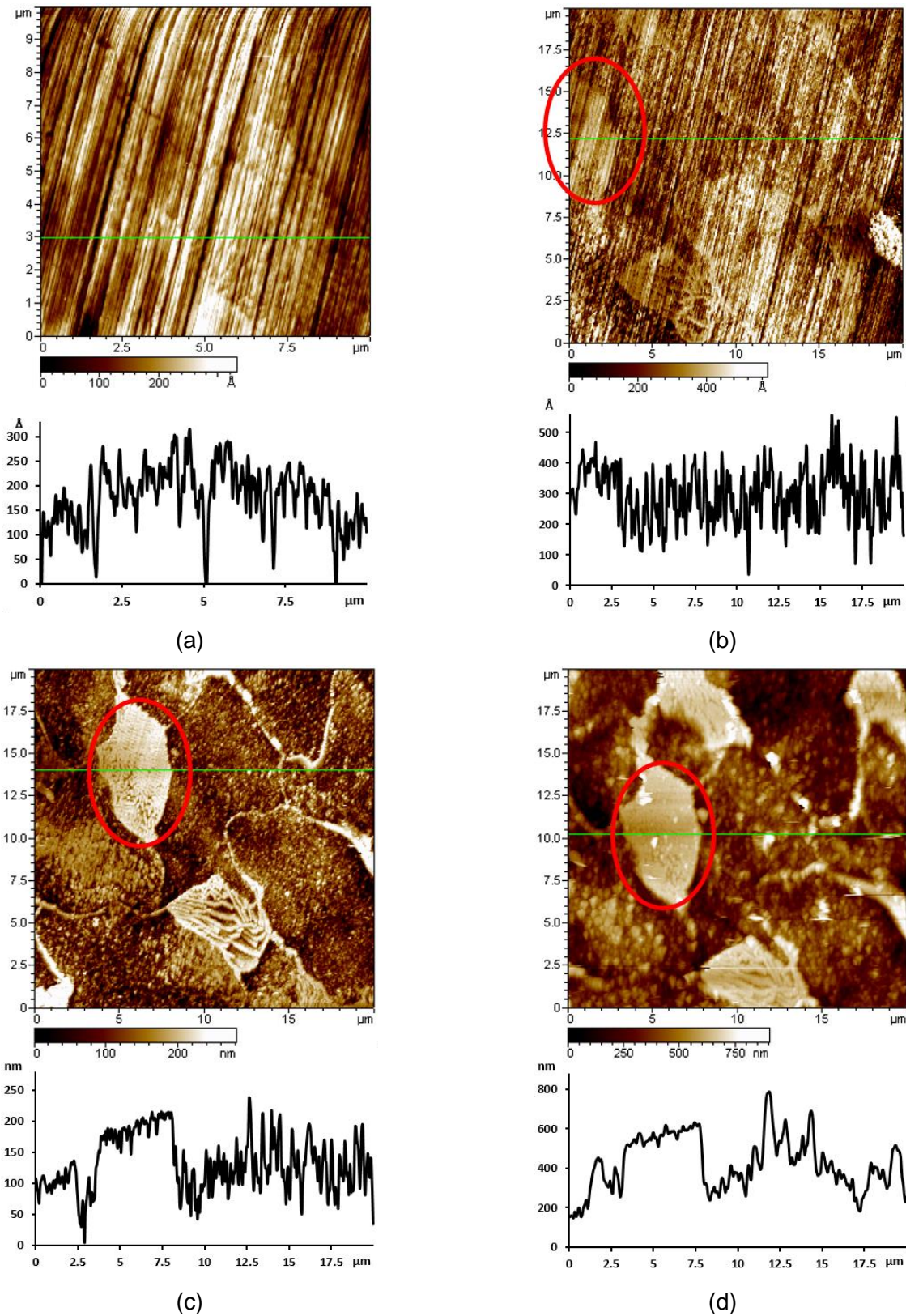


**Figure 5. Real time monitoring of UNS G10180 steel morphology by AFM : (a) in air, (b-d) in a 1 wt% NaCl aqueous solution after b) 10 minutes (c) 1 hour (d) 4 hours immersion times.**

## Real time monitoring of steel surface morphology in the presence of Q-C14 inhibitor at a 0.5 CMC bulk concentration

A sequence of in situ AFM morphology images were also collected on the same steel surface at various immersion times in 1wt% NaCl aqueous solution in the presence of Q-C14 inhibitor at various concentrations, as shown in Figure 6 through Figure 10.

At the 0.5 CMC bulk concentration, there were regions of the surface that were protected and others that were not. Figure 6 displays the morphology images of a typical unprotected regions on steel surface and reveals a corrosion behavior similar to the one observed in an aqueous solution in the absence of inhibitor (Figure 5). As presented in Figure 6b and Figure 6c, sustained corrosion of the ferrite phase was revealed by the continuous decrease of surface height in the ferrite region with time, while at the same time the cementite structures were conserved as on the original steel surface. Based on the topography profiles in Figure 6 a-c, the height differences between pearlite structure and surrounding ferrite are about  $16 \pm 8$  nm,  $90 \pm 30$  nm, and  $300 \pm 60$  nm respectively after immersion in the 0.5 CMC inhibitor solution for 10 minutes, 1 hour and 4 hours. It is estimated from these height difference values and Equation (1) that the corrosion rate between 10 minutes to 1 hour is  $0.78 \pm 0.23$  mm/year and the time averaged local corrosion rate from 1 hour to 4 hours exposure is estimated as  $0.61 \pm 0.26$  mm/year, which are in the same magnitude of the surface averaged corrosion rate as estimated by AFM topography profile in uninhibited solution. It could be therefore inferred that this region was not protected by the inhibitor at all, because it was either not covered by the inhibitor or was covered by an unstructured inhibitor layer that offered little or no protection.

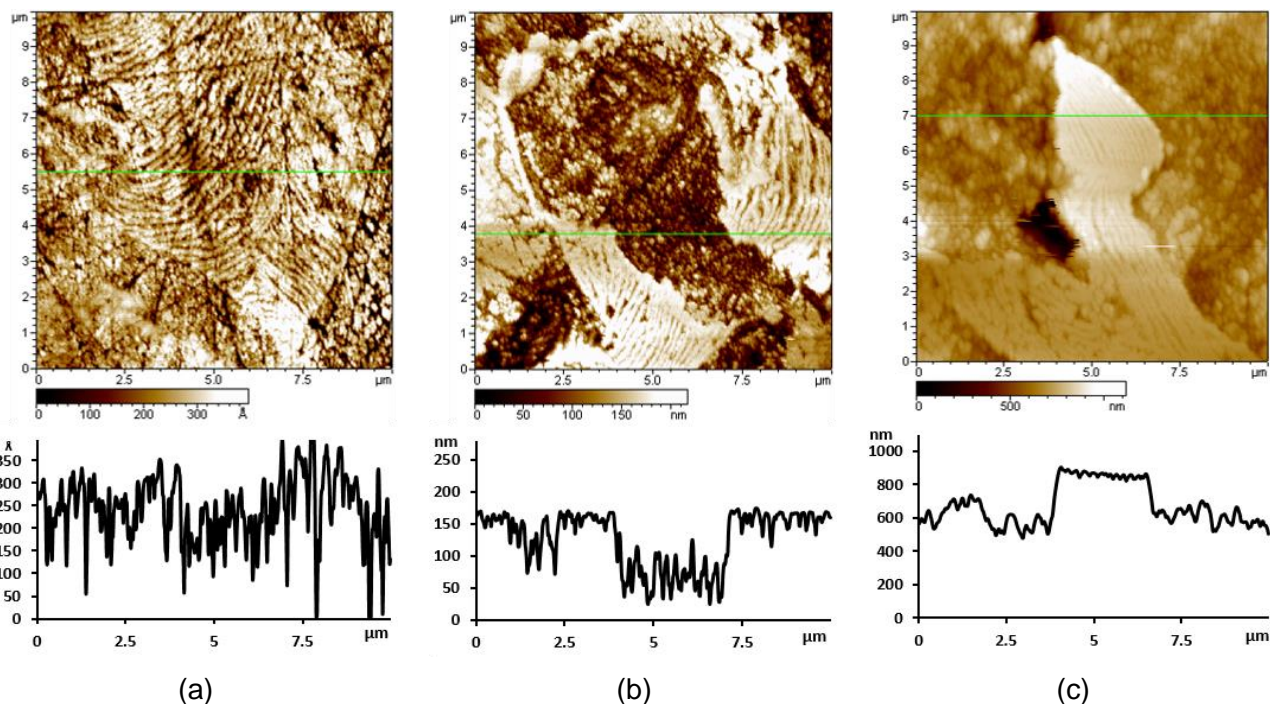


**Figure 6. Real time monitoring of UNS G10180 steel morphology (case of an unprotected region) by AFM (a) in air, (b-c) in a 1 wt% NaCl aqueous solution in the presence of Q-C14 at 0.5 CMC after (b) 10 minutes (c) 4 hours immersion time.**

Figure 7 shows an example of the surface morphology of an inhibited region in the presence of Q-C14 at a 0.5 CMC bulk concentration. Figure 7a shows the mild steel surface before immersion in the aqueous solution. After 10 minutes in this solution, slight corrosion of  $\alpha$  - Fe has occurred as revealed by the appearance of cementite stripes. Nevertheless, there was no further obvious change of surface morphology with an increased immersion time of 4 hours, as can be observed in Figure 7c.

The slight corrosion in Figure 7b after 10 minutes can be attributed to the kinetic limitation of inhibitor adsorption. Within the first few minutes after adding inhibitor solution on steel surface, the inhibitor took some time to adsorb on the steel surface and form a SAM, so that in this period the anodic ferrite corroded somewhat, leaving the striped cementite behind(Figure 7b).

Obviously, between 10 minutes and 4 hours we cannot see any further changes in the steel surface and can safely assume that in this period the inhibitor adsorbed on this part of the steel surface and formed a SAM, which minimized further dissolution of the ferrite phase.

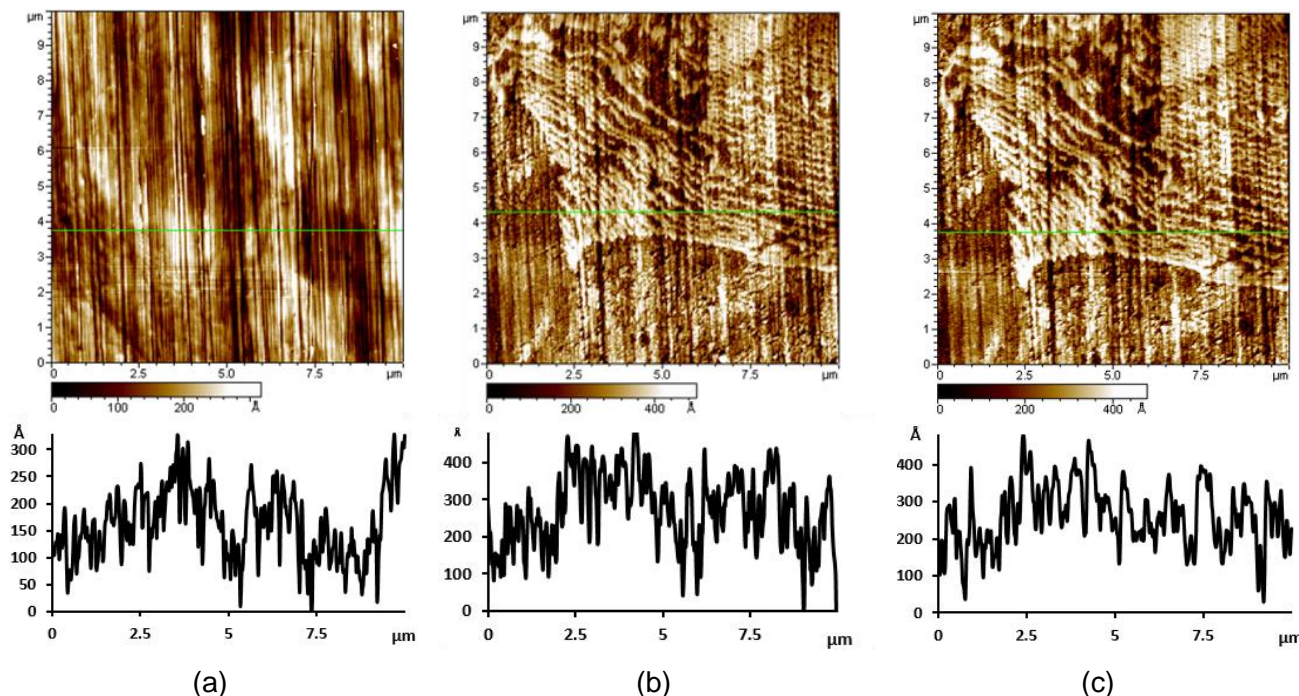


**Figure 7. Real time monitoring for UNS G10180 steel morphology (case of a protected region) by AFM (a) in air, (b-c) in a 1 wt% NaCl aqueous solution in the presence of Q-C14 at 0.5 CMC after (b) 10 minutes, (c) 4 hours immersion time.**

Based on the AFM images at 0.5 CMC bulk concentration, patchy coverage by the inhibitor was indicated on the mild steel surface. Multiple experiments have been conducted in order to establish repeatability.

Due to the high resolution of the AFM it was difficult to estimate the size of these protected and unprotected regions on the steel surface. Therefore, after the AFM experiments, the steel samples exposed for 4 hours in the 0.5 CMC solution were transferred to a SEM for surface observations. Figure 8a shows an example of the morphology of an unprotected region at approximately the same magnification as was used in the AFM images above. Similar morphology is indicated with serious corrosion of the ferrite phase and the cementite structures remaining unchanged. The SEM image of a protected region (Figure 8b) indicates some slight corrosion by the appearance of the cementite structure. However, polishing lines can still be seen clearly on the steel surface, revealing that further dissolution of ferrite was prevented in longer exposure (4 h). The SEM image obtained at a lower magnification (Figure 8c) indicates a boundary between an unprotected (highly corroded) region and a protected (barely corroded) region, confirming the patchy protection behavior of Q-C14 at 0.5 CMC concentration on UNS G10180 steel surface. The size of these patches was in the range of a 0.1 – 1 mm.

This patchy protection phenomenon was consistent with previous in-situ AFM studies of surfactants adsorption mechanisms on mica showing two different stages<sup>11, 13, 14</sup>. In the initial induction period, a rapid adsorption of Q-C14 at mica surface is driven by an electrostatic attraction between the positive Q-C14

and the negative lattice sites on mica. The initial adsorption sites are random and unpredictable. In order to accomplish nucleation, subsequent inhibitor molecules were more prone to adsorb on these initial sites. After this nucleation process, a loosely packed sub-monolayer of adsorbed Q-C14 formed on the surface as islands, which then grew and coalesced together. Meanwhile, initially randomly unselected sites remained uncovered due to the equilibrium established at this low concentration (0.5 CMC). It was therefore expected that at higher concentrations (1 and 2 CMC shown below), the excess inhibitor molecules in the bulk solution will be able to cover up the initially uncovered sites and approach full coverage.

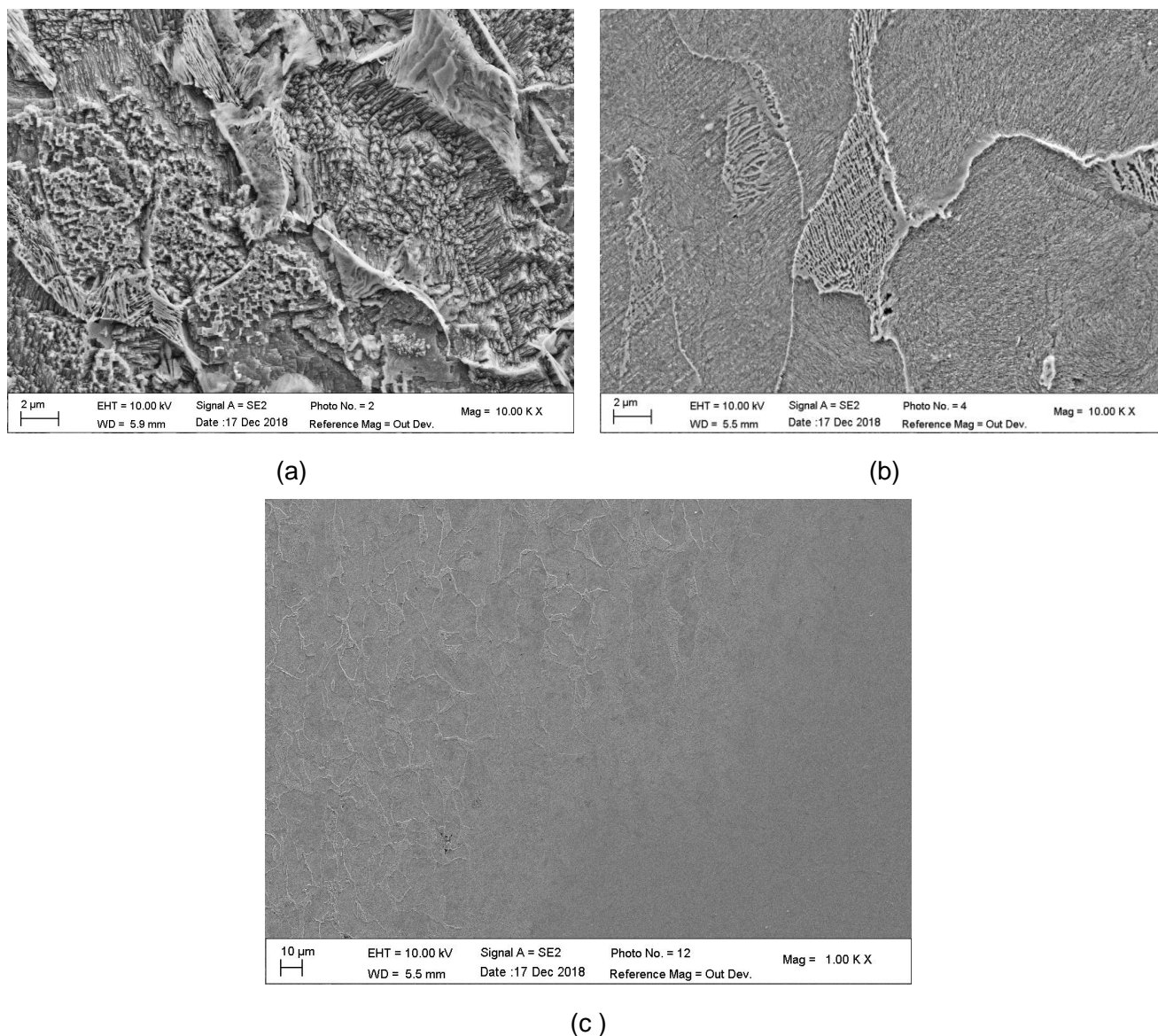


**Figure 8. Ex-situ SEM images of the sample used for in-situ AFM imaging (see Figure 6 and Figure 7) after a 4 hours immersion in a 1 wt% NaCl aqueous solution containing Q-C14 (0.5 CMC) (a) unprotected region, (b) protected region, (c) a boundary between unprotected and protected regions.**

### **Real time monitoring using in-situ AFM in the presence of Q-C14 inhibitor at a 1 CMC bulk concentration**

©2020 by NACE International.

Requests for permission to publish this manuscript in any form, in part or in whole, must be in writing to NACE International, Publications Division, 15835 Park Ten Place, Houston, Texas 77084.

The material presented and the views expressed in this paper are solely those of the author(s) and are not necessarily endorsed by the Association.

Figure 9 displays the surface morphology of UNS G10180 steel with Q-C14 at 1 CMC concentration. Multiple images on different locations of the same steel surface showed that no serious or sustained corrosion could be seen. The steel surface morphology at the end of the experiment either showed slight corrosion (Figure 9b and Figure 9c) or no corrosion – it preserved the same morphology as in air. This implies that at a 1 CMC concentration, the Q-C14 inhibitor achieved full coverage on the steel surface by forming a protective SAM. The slight discrepancies seen in morphology on different parts of the surface (slight corrosion vs. no corrosion at all) may depend on the nucleation and SAM formation at different locations on the surface. Considering that this initial stage of adsorption was short (less than 10 minutes), after which full inhibitor coverage reduced the corrosion rate to an extremely low value over the entire surface of the sample, only small variations in the surface morphology are seen. However, as shown by LPR corrosion rate results (Figure 4), corrosion still continued albeit at an extremely low rate (of the order of 0.1 mm/year). This translates into a total of approximately 1  $\mu\text{m}$  over the 4 days, something that could not be clearly identified in the AFM images.

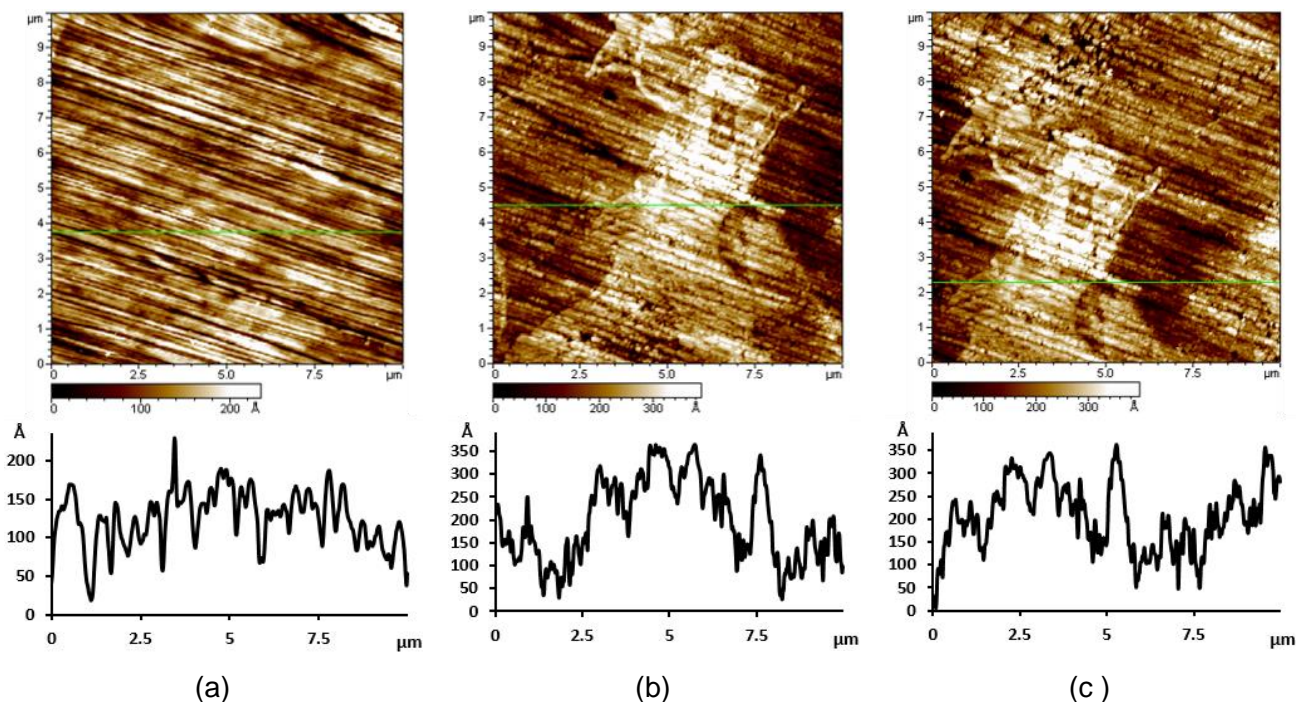


**Figure 9. Real time monitoring of UNS G10180 steel morphology (case of a protected region) by AFM (a) in air, (b-c) in a 1 wt% NaCl aqueous solution in the presence of Q-C14 at 1 CMC after (b) 10 minutes, (c) 4 hours immersion time.**

### Real time monitoring using in-situ AFM in the presence of Q-C14 inhibitor at a 2 CMC bulk concentration

Figure 10 displays the surface morphology of mild steel imaged using in-situ AFM in the presence of Q-C14 inhibitor at a 2 CMC bulk concentration. The morphology is similar with that observed at 1 CMC. If one assumes that the adsorption of inhibitor reached a full coverage with protective SAM at 1 CMC as deduced from the corrosion behavior observed in Figure 9, then it is logical that the same was also obtained at 2 CMC. This is consistent with the LPR measurements shown in Figure 4, where similar final corrosion rate was measured for both 0.5 and 1 CMC.

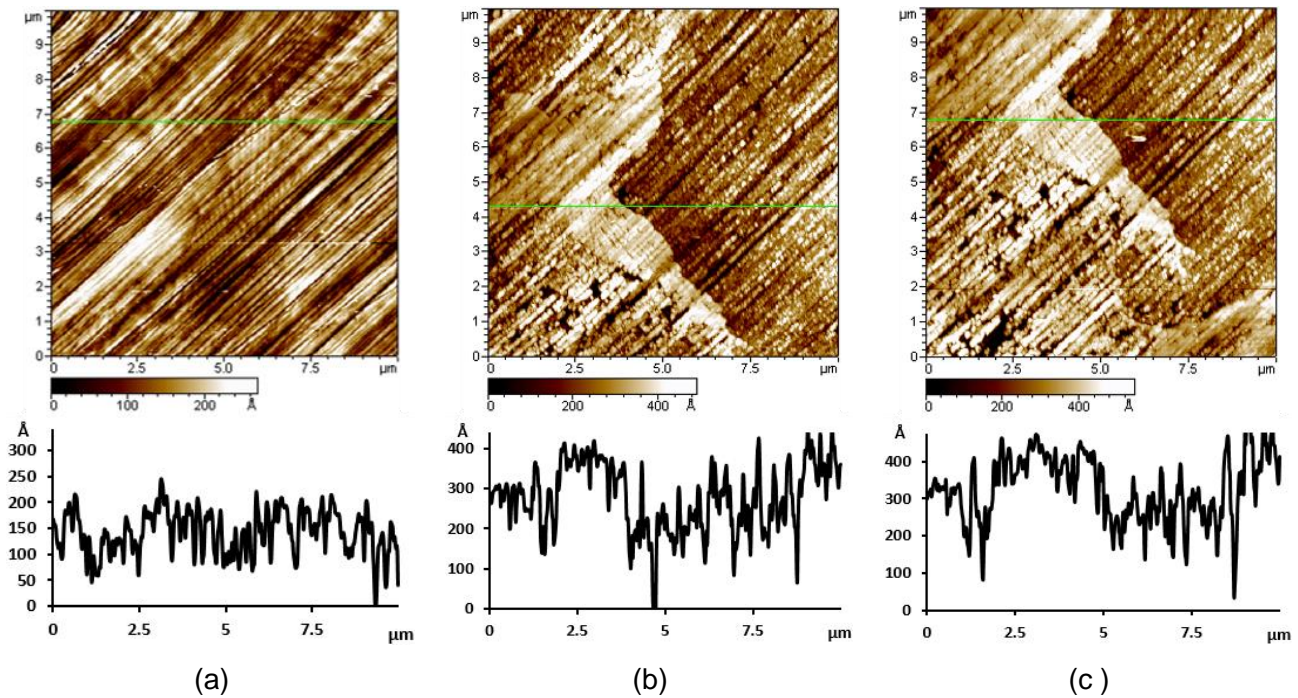


**Figure 10. Real time monitoring of UNS G10180 steel morphology (case of a protected region) by AFM (a) in air, (b-c) in a 1 wt% NaCl aqueous solution in the presence of Q-C14 at 2 CMC after (b) 10 minutes, (c) 4 hours immersion time.**

## CONCLUSIONS

The investigation of adsorption structure and inhibition efficiency for corrosion inhibitor Q-C14 using AFM imaging and in-situ LPR measurements revealed that, for UNS G10180 steel in a 0.5 CMC inhibitor concentration (25 ppm) of aqueous solution, patchy corrosion protection occurred. Some areas of the steel surface were covered with inhibitor within 10 minutes, while other parts of the steel surface corroded continuously and more quickly as if they were not covered with an inhibitor layer. Partial coverage of inhibitor could lead to localized corrosion. For UNS G10180 steel in a Q-C14 inhibitor aqueous solution at 1 and 2 CMC concentrations (100 ppm), the entire surface was covered with inhibitor and low corrosion rates were obtained.

## ACKNOWLEDGEMENTS

The authors would like to thank the following companies for their financial support: Anadarko, Baker Hughes, BP, Chevron, CNOOC, ConocoPhillips, DNV GL, ExxonMobil, M-I SWACO (Schlumberger), Multi-Chem (Halliburton), Occidental Oil Company, Saudi Aramco, Shell Global Solutions, SINOPEC (China Petroleum), and TOTAL.

The authors also express their gratitude to the National Science Foundation.

## REFERENCES

- [1] A.M. Al - Sabbagh, M.M. Osman, A.M.A. Omar, I.M. El - Gamal, "Organic corrosion inhibitors for steel pipelines in oilfields," *Anti-corrosion methods and materials* 43, 6 (1996): p.11-16.
- [2] A.M. Alsabagh, M.A. Migahed, H.S. Awad, "Reactivity of polyester aliphatic amine surfactants as corrosion inhibitors for carbon steel in formation water (deep well water)," *Corrosion Science* 48, 4 (2006) : p. 813-828.

- [3] D. Özkır, K. Kayakırılmaz, E. Bayol, A.A. Gürten, F. Kandemirli, "The inhibition effect of Azure A on mild steel in 1 M HCl, A complete study: Adsorption," temperature, duration and quantum chemical aspects," *Corrosion Science* 56, 1 (2012) : p.143-152.
- [4] M. Gopiraman, N. Selvakumaran, D. Kesavan, R. Karvembu, "Adsorption and corrosion inhibition behaviour of N-(phenylcarbamothioyl) benzamide on mild steel in acidic medium," *Progress in Organic Coatings* 73, 1 (2012) :p.104-111.
- [5] M.G. Fontana, *Corrosion engineering*, 3<sup>rd</sup> ed. (United States:Tata McGraw-Hill Education, 1986), p. 52.
- [6] X. Chen, W. Dong, X. Zhang, "Self-assembly of amphiphilic molecules: A review on the recent computer simulation results," *Science China Chemistry* 53, 9 (2010):p.1853-1861.
- [7] H.N. Patrick, G.G. Warr, S. Manne, I.A. Aksay, "Surface micellization patterns of quaternary ammonium surfactants on mica," *Langmuir* 15, 5(1999): p.1685-1692.
- [8] S. Manne, T. Schäffer, Q. Huo, P. Hansma, D. Morse, G. Stucky, I. Aksay, "Gemini surfactants at solid– liquid interfaces: control of interfacial aggregate geometry," *Langmuir* 13, 24(1997):p. 6382-6387.
- [9] X. Ko, S. Sharma, "Adsorption and Self-Assembly of Surfactants on Metal–Water Interfaces," *The Journal of Physical Chemistry B* 121, 45(2017) 10364-10370.
- [10] S. Sharma, X. Ko, Y. Kurapati, H. Singh, S. Nešić, "Adsorption Behavior of Organic Corrosion Inhibitors on Metal Surfaces—Some New Insights from Molecular Simulations," *Corrosion* 75, 1(2018):p. 90-105.
- [11] J. Woodward, I. Doudevski, H. Sikes, D. Schwartz, "Kinetics of self-assembled monolayer growth explored via submonolayer coverage of incomplete films," *The Journal of Physical Chemistry B* 101, 38(1997) :p.7535-7541.
- [12] D. Schwartz, S. Steinberg, J. Israelachvili, J. Zasadzinski, "Growth of a self-assembled monolayer by fractal aggregation," *Physical review letters* 69, 23(1992):p. 3354.
- [13] I. Doudevski, W.A. Hayes, D.K. Schwartz, "Submonolayer island nucleation and growth kinetics during self-assembled monolayer formation," *Physical review letters* 81 , 22(1998) 4927.
- [14] W.A. Hayes, D.K. Schwartz, "Two-stage growth of octadecyltrimethylammonium bromide monolayers at mica from aqueous solution below the Krafft point," *Langmuir* 14, 20(1998):p. 5913-5917.
- [15] M. Jaschke, H.J. Butt, H.E. Gaub, S. Manne, "Surfactant Aggregates at a Metal Surface," *Langmuir* 13, 13(1997):p.1381-1384.
- [16] G.E. Poirier, E.D. Pylant, "The Self-Assembly Mechanism of Alkanethiols on Au(111)," *science* 272, 5265(1996):p. 1145-1148.
- [17] J.D. Olivo, B. Brown, S. Nestic, "Modeling of corrosion mechanisms in the presence of quaternary ammonium chloride and imidazoline corrosion inhibitors," CORROSION/2016, paper no.7406( Houston, TX:NACE, 2016), p. 1.
- [18] J.D. Olivo, D. Young, B. Brown, S. Nestic, "Effect of Corrosion Inhibitor Alkyl Tail Length on the Electrochemical Process Governing CO<sub>2</sub> Corrosion of Mild Steel," *Corrosion* 75, 2(2019) :p.137-139.
- [19] A.a.F. Eftaiha, M.F. Paige, "The influence of salinity on surfactant miscibility in mixed dipalmitoylphosphatidylcholine–perfluorooctadecanoic acid monolayer films," *Journal of colloid and interface science* 353, 1(2011):p. 210-219.
- [20] Y. Xiong, B. Brown, B. Kinsella, S. Nestic, A. Pailleret, "AFM studies of the adhesion properties of surfactant corrosion inhibitor films," in: CORROSION/2013, paper no. 2521 (Houston, Texas : NACE, 2013), p.1.
- [21] Z. Belarbi, B. Brown, M. Singer, N. Srdjan, "Study of Adsorption of Corrosion Inhibitor 1-(2-aminoethyl)-2-oleyl-2-imidazolium Chloride on Carbon Steel Under CO<sub>2</sub> Environment by Using In-Situ AFM Measurements," in: CORROSION/2017, paper no. 9290 ( Houston, TX:NACE, 2017), p. 1.
- [22] W. Li, B. Pots, X. Zhong, S. Nestic, "Inhibition of CO<sub>2</sub> corrosion of mild steel– Study of mechanical effects of highly turbulent disturbed flow," *Corrosion Science* 126, 1 (2017):p. 208-226.
- [23] T. Murakawa, S. Nagaura, N. Hackerman, "Coverage of iron surface by organic compounds and anions in acid solutions," *Corrosion Science* 7, 2(1967):p. 79-89.
- [24] N. Pebere, M. Duprat, F. Dabosi, A. Lattes, A. De Savignac, "Corrosion inhibition study of a carbon steel in acidic media containing hydrogen sulphide and organic surfactants," *Journal of Applied Electrochemistry* 18, 2 (1988) :p. 225-231.

- [25] J. Bulger, B. Lu, J. Luo, "Microstructural effect on near-neutral pH stress corrosion cracking resistance of pipeline steels," *Journal of materials science* 41, 15 (2006): p. 5001-5005.
- [26] Y. Ivanisenko, W. Lojkowski, R. Valiev, H.-J. Fecht, "The mechanism of formation of nanostructure and dissolution of cementite in a pearlitic steel during high pressure torsion," *Acta Materialia* 51, 18(2003):p. 5555-5570.
- [27] L.D. Paolinelli, T. Pérez, S.N. Simison, "The effect of pre-corrosion and steel microstructure on inhibitor performance in CO<sub>2</sub> corrosion," *Corrosion Science* 50, 9 (2008): p.2456-2464.
- [28] B. Mishra, S. Al-Hassan, D. Olson, M. Salama, "Development of a predictive model for activation-controlled corrosion of steel in solutions containing carbon dioxide," *Corrosion* 53, 11(1997) :p. 852-859.
- [29] F. Farelas, B. Brown, S. Nestic, "Iron carbide and its influence on the formation of protective iron carbonate in CO<sub>2</sub> corrosion of mild steel," in: CORROSION/2013, paper no. 2291 ( Houston, TX: NACE, 2017), p. 1.
- [30] Z. Zhang, G. Chen, G.J.M.S. Chen, E. A, "Microstructural evolution of commercial pure iron during directional annealing," *Materials Science and Engineering: A* 422, 1-2 (2006) :p. 241-251.